IEEE Access
Multidisciplinary ⋮ Rapid Review ⋮ Open Access Journal

Received 22 December 2023, accepted 28 December 2023, date of publication 2 January 2024, date of current version 10 January 2024.

Digital Object Identifier 10.1109/ACCESS.2023.3349271

RESEARCH ARTICLE

Barrier Function-Based Adaptive Super-Twisting Integral Terminal Sliding Mode Control for a Quad-Rotor UAV

XINXIN CHEN
School of Electrical and Electronic Engineering, Guangdong Technology College, Zhaoqing 526110, China
e-mail: xxchen127@163.com

This work was supported in part by the Guangdong Province Online and Offline Hybrid First-Class Courses under Grant 2021-328, and in part by the Guangdong University Teaching Quality and Teaching Reform Project Construction Project 2020-19.

ABSTRACT In this paper, a novel barrier function-based super-twisting integral terminal sliding mode control algorithm is proposed for a quad-rotor unmanned aerial vehicle (UAV). The approach of employing an integral terminal sliding mode control strategy is adopted to achieve an equivalent control, while the switching control law is designed using the super-twisting algorithm. The barrier function is introduced as the gain of switching control law. The integral terminal sliding mode approach guarantees that the system's initial state lies on the sliding mode surface, while also enhancing the convergence rate of the system state through exponential acceleration. Super-twisting algorithm is introduced to reduce the sliding mode chattering. The barrier function can guarantee the convergence of output variables and induce a decrease in gain proportionate to the output variables. Finally, the numerical simulation results demonstrate the efficacy and exceptional performance of the proposed schemes.

INDEX TERMS Integral terminal sliding mode control, super-twisting algorithm, barrier function, quad-rotor UAV.

I. INTRODUCTION

In recent years, quad-rotor UAVs have been widely used in military and civilian fields such as military reconnaissance [1], power inspection [2], agriculture [3], and forest fire control [4] and so on due to their advantages of small fuselage and flexible movement. With the diversification and complexity of applications for quad-rotor UAV [5], [6], there is a high demand placed on their control performance. There are two crucial objectives in the design of a quad-rotor UAV controller: achieving precise attitude control by managing the angles of the quad-rotor UAV and implementing effective height control to position it advantageously. Because the quad-rotor UAV system is highly nonlinear, it is a big challenging research to achieve accurate control.

In previous work, there has been literature that has proposed various quad-rotor UAV control methods such as robust control [7], fuzzy control [8], adaptive neural network [9], backstepping [10] and sliding mode control. Due to its simplicity, fast response speed, and robustness against external noise interference and parameter perturbations, the sliding mode control algorithm is often applied in quad-rotor UAV control [11], [12], [13]. In the past few years, remarkable control performance has been exhibited by integral terminal sliding mode control [14], [15], [16]. The integral terminal sliding mode control exhibits remarkable attributes including excellent robustness, rapid response speed, and finite time convergence. Compared to conventional terminal sliding mode control, integral terminal sliding mode control can achieve finite-time convergence of tracking error and integration error without encountering singularity issues [17].

However, in terms of chattering suppression, the performance of integral terminal sliding mode control is often unsatisfactory. In order to weaken the chattering of the integral terminal sliding mode, the super-twisting algorithm [18] is introduced to solve this problem. The super-twisting algorithm is widely used to design controllers

The associate editor coordinating the review of this manuscript and approving it for publication was Zhiguang Feng.

due to their excellent finite-time convergence [19], [20], [21]. However, the gain of the super-twisting cannot be updated in real-time with the system state, which is easy to cause instability of the control state. Therefore, the barrier function is introduced as the gain of the super-twisting algorithm. The barrier function guarantees the convergence of output variables and maintains them within a predefined vicinity of zero. Furthermore, because of the unique structure of the barrier function, it compels the gain to decrease in tandem with the output variable, thereby enhancing control performance.

The primary aim of these methods is to adaptively modify the control gains to minimize them to the greatest extent possible, while still ensuring adequate mitigation of disturbances. One approach to mitigate these disruptions is by adjusting the gain to guarantee the attainment of the sliding mode. Once the sliding mode is reached, the high-frequency control signal is subjected to filtration and utilized for extracting information regarding perturbations in the controller's gain. The gain of the sliding mode controller is calculated by adding the filtered signal to a constant value, which serves to offset any possible differences between the actual disturbance and its estimated value derived from filtering. However, a prerequisite for this is having knowledge of the minimum and maximum acceptable values for the adaptive gain. According to these methods, the gain progressively rises until the sliding mode is attained, and subsequently declines when the sliding mode is no longer maintained, indicating a deviation from the desired state. These approaches ensure that the sliding variable converges to a neighborhood around zero within a finite time, without significantly overestimating the gain.

The main contributions of this paper are listed as follows:

- A novel adaptive super-twisting integral terminal sliding mode controller based on barrier function is proposed for the quad-rotor UAV with external disturbance.
- Robust adaptive finite-time fast convergence stabilizer and tracker design for a quad-rotor UAV system.
- The quad-rotor UAV often encounters various unestimable disturbances in the actual use process, such as the wind. Disturbances due to wind are often unpredictable. However, this algorithm does not require an upper bound of the disturbance derivative, which ensures that once the derivative of the perturbation increases, the supertwist gain also increases. When the gain is sufficiently large to guarantee convergence to the origin, the barrier function strategy compels a decrease in the supertwist gain along with the output variable, thereby avoiding any detrimental effects caused by excessive gain.

The remaining structure of this paper is as follows: Section II introduces the dynamics modeling of quad-rotor UAV based on state space. In Section III, problem description and some preparatory work are given. In Section IV, the designed sliding surface and control law are presented, as well as the stability proof. A simulation experiment is used to verify the effectiveness of the proposed approach in Section V. Finally, the conclusion of this paper and future prospects are given in Section VI.

II. DYNAMICS MODEL OF QUAD-ROTOR UAV

A quad-rotor system consists of four rotors that provide different directions of turning and movement by adjusting the total thrust, either increasing or decreasing it. In order to establish a quad-rotor UAV model, the following assumptions are made:

- The propellers have a rigid structure.
- The structure of the quad-rotor is both rigid and symmetrical.
- The correlation between propeller velocity and thrust and drag is characterized by a direct proportionality to the square of each other.

Based on the assumptions and equations proposed by Newton-Euler, we can express the dynamic equation of a quad-rotor UAV in the following manner:

$$\begin{cases} m\ddot{\zeta} = F_f + F_d + F_g \\ J\dot{\Omega} = -\Omega^T J\Omega + \Gamma_f + \Gamma_a + \Gamma_g \end{cases} \tag{1}$$

where ζ is the position of the quad-rotor's center of mass relative to the center of inertia. m is the mass of a quad-rotor UAV. $J \in \mathbf{R}^{3\times 3}$ is the symmetric positive-definite constant inertia matrix. J is represented as follows:

$$J = \begin{bmatrix} I_x & 0 & 0 \\ 0 & I_y & 0 \\ 0 & 0 & I_z \end{bmatrix} \tag{2}$$

where $I_i(i = x, y, z)$ is inertia values respect to x, y and z axis. Ω represents the angular velocity of the quad-rotor UAV. The expression is as follows:

$$\Omega = \begin{bmatrix} 1 & 0 & -sin\theta \\ 0 & cos\phi & cos\theta sin\phi \\ 0 & -sin\phi & cos\theta cos\phi \end{bmatrix} \begin{bmatrix} \dot{\phi} \\ \dot{\theta} \\ \dot{\psi} \end{bmatrix} \tag{3}$$

where θ, ψ, ϕ are pitch, yaw and roll angles, respectively. F_f denotes the total of the forces produced by the four propellers, it can be expressed as follows

$$F_f = \begin{bmatrix} cos\phi cos\psi sin\theta + sin\phi sin\psi \\ cos\phi sin\theta sin\psi - sin\phi cos\psi \\ cos\theta cos\phi \end{bmatrix} \sum_{i=1}^{4} F_i \tag{4}$$

while $F_i = K_p\omega_i^2$. K_p is related to lift. ω_i represents the angular velocity of the four rotors. F_d denotes the composite force acting along the X, Y, and Z axes.

$$F_d = \begin{bmatrix} -K_{fdx} & 0 & 0 \\ 0 & -K_{fdy} & 0 \\ 0 & 0 & -K_{fdz} \end{bmatrix} \dot{\zeta} \tag{5}$$

where K_{fdx}, K_{fdy} and K_{fdz} are positive translation drag coefficients. The gravity matrix F_g could be expressed as follows:

$$F_g = \begin{bmatrix} 0 \\ 0 \\ -mg \end{bmatrix} \tag{6}$$

where g represents the gravity. Γ_f represents the torque generated by the four rotors as:

$$\Gamma_f = \begin{bmatrix} d(F_3 - F_1) \\ d(F_4 - F_2) \\ C_d(\omega_1^2 - \omega_2^2 + \omega_3^2 - \omega_4^2) \end{bmatrix} \tag{7}$$

where d and C_D denote the distance between the propeller's axis of rotation and the center of the quad-rotor UAV, as well as its drag coefficient. Γ_a represents the outcome of aerodynamic friction torques, it can be expressed as follows:

$$\Gamma_a = \begin{bmatrix} K_{fax} & 0 & 0 \\ 0 & K_{fay} & 0 \\ 0 & 0 & K_{faz} \end{bmatrix} \|\Omega\|^2 \tag{8}$$

where K_{fax}, K_{fay} and K_{faz} denote the aerodynamic friction coefficients. Γ_a represents the resultant of torques caused by the gyroscopic effect and it is expressed as follows:

$$\Gamma_g = \sum_{i=1}^{4} \Omega^T J_r \begin{bmatrix} 0 \\ 0 \\ (-1)^{i+1}\omega_i \end{bmatrix} \tag{9}$$

where J_r denotes the rotor inertia. The dependence of the control law on the angular velocity of the propeller is expressed as follows:

$$\begin{bmatrix} u_1 \\ u_2 \\ u_3 \\ u_4 \end{bmatrix} = \begin{bmatrix} K_p & K_p & K_p & K_p \\ -K_p & 0 & K_p & 0 \\ 0 & -K_p & 0 & K_p \\ C_D & -C_D & C_D & -C_D \end{bmatrix} \begin{bmatrix} \omega_1^2 \\ \omega_2^2 \\ \omega_3^2 \\ \omega_4^2 \end{bmatrix} \tag{10}$$

where $u_i(i = 1, 2, 3, 4)$ denotes the control singles. $\omega_i(i = 1, 2, 3, 4)$ is the angular velocity, it can be expressed as follows:

$$\begin{bmatrix} \omega_1 \\ \omega_2 \\ \omega_3 \\ \omega_4 \end{bmatrix} = \left(\begin{bmatrix} K_p & K_p & K_p & K_p \\ -K_p & 0 & K_p & 0 \\ 0 & -K_p & 0 & K_p \\ C_D & -C_D & C_D & -C_D \end{bmatrix}^{-1} \begin{bmatrix} u_1 \\ u_2 \\ u_3 \\ u_4 \end{bmatrix} \right)^{\frac{1}{2}} \tag{11}$$

The dynamics model of a quad-rotor UAV can be expressed as follows:

$$\begin{cases} \ddot{x} = \dfrac{1}{m}[-K_{fdx}\dot{x} + (cos\phi sin\theta cos\psi + sin\phi sin\psi)u_1] \\ \ddot{y} = \dfrac{1}{m}[-K_{fdy}\dot{y} + (cos\phi sin\theta sin\psi - sin\phi sin\psi)u_1] \\ \ddot{z} = \dfrac{1}{m}[-K_{fdz}\dot{z} + (cos\phi cos\theta)u_1] - g \\ [0.5pc]\ddot{\phi} = \dfrac{1}{I_x}[(I_y - I_z)\dot{\psi}\dot{\theta} - K_{fax}\dot{\phi}^2 - J_r\bar{\Omega}\dot{\theta} + du_2] \\ \ddot{\theta} = \dfrac{1}{I_y}[(I_z - I_x)\dot{\psi}\dot{\phi} - K_{fay}\dot{\theta}^2 + J_r\bar{\Omega}\dot{\phi} + du_3] \\ \ddot{\psi} = \dfrac{1}{I_z}[(I_x - I_y)\dot{\phi}\dot{\theta} - K_{faz}\dot{\psi}^2 + C_D u_4] \end{cases} \tag{12}$$

where $\bar{\Omega} = \omega_1 - \omega_2 + \omega_3 - \omega_4$.

III. PROBLEM STATEMENT AND PRELIMINARIES

Considering $\dot{x}_i = \left[\dot{\phi}, \ddot{\phi}, \dot{\theta}, \ddot{\theta}, \dot{\psi}, \ddot{\psi}, \dot{z}, \ddot{z}\right]^T$ $(i = 1 \ldots 8)$ are the system states. The state space equation of Eq. (12) is expressed as follows

$$\begin{cases} \dot{x}_1 = x_2 \\ \dot{x}_2 = a_1x_4x_6 + a_2x_2^2 + a_3\bar{\Omega}x_4 + b_1u_2 + d_\phi(t) \\ \dot{x}_3 = x_4 \\ \dot{x}_4 = a_4x_2x_6 + a_5x_4^2 + a_6\bar{\Omega}x_2 + b_2u_3 + d_\theta(t) \\ \dot{x}_5 = x_6 \\ \dot{x}_6 = a_7x_2x_4 + a_8x_6^2 + b_3u_4 + d_\psi(t) \\ \dot{x}_7 = x_8 \\ \dot{x}_8 = a_9x_8 - g + \dfrac{cosx_1cosx_3}{m}u_1 + d_z(t) \end{cases} \tag{13}$$

where $u_i(i = 1, 2, 3, 4)$ are the control singles and $d_j(j = \phi, \theta, \psi, z)$ are external disturbances with $a_1 = \frac{I_y - I_z}{I_x}$, $a_2 = \frac{-K_{fax}}{I_x}$, $a_3 = \frac{-J_r}{I_x}$, $a_4 = \frac{I_z - I_x}{I_y}$, $a_5 = \frac{-K_{fay}}{I_y}$, $a_6 = \frac{J_r}{I_y}$, $a_7 = \frac{I_x - I_y}{I_z}$, $a_8 = \frac{-K_{faz}}{I_z}$, $a_9 = \frac{-K_{fdz}}{m}$, $b_1 = \frac{d}{I_x}$, $b_2 = \frac{d}{I_y}$, $b_3 = \frac{C_D}{I_z}$.

The error between the expected and the actual value and the first derivative of the error are defined as follows:

$$\begin{aligned} &e_1 = x_1 - x_{1d}, e_2 = x_3 - x_{2d} \\ &e_3 = x_5 - x_{3d}, e_4 = x_7 - x_{4d} \end{aligned} \tag{14}$$

$$\begin{aligned} &\dot{e}_1 = \dot{x}_1 - \dot{x}_{1d}, \dot{e}_2 = \dot{x}_3 - \dot{x}_{2d} \\ &\dot{e}_3 = \dot{x}_5 - \dot{x}_{3d}, \dot{e}_4 = \dot{x}_7 - \dot{x}_{4d} \end{aligned} \tag{15}$$

$$\begin{aligned} &\ddot{e}_1 = \ddot{x}_1 - \ddot{x}_{1d}, \ddot{e}_2 = \ddot{x}_3 - \ddot{x}_{2d} \\ &\ddot{e}_3 = \ddot{x}_5 - \ddot{x}_{3d}, \ddot{e}_4 = \ddot{x}_7 - \ddot{x}_{4d} \end{aligned} \tag{16}$$

where $x_{id}(i = 1, 2, 3, 4)$ is the expected trajectory, $\dot{x}_{id}(i = 1, 2, 3, 4)$ is the first derivative of the expected trajectory and $\ddot{x}_{id}(i = 1, 2, 3, 4)$ is the second derivative of the expected trajectory.

Definition 1 [22]: $\varepsilon > 0$ is fixed and given. For any positive real number b, a barrier function can be defined as a continuous function $L_b(x) : x \in (-\varepsilon, \varepsilon)$ such that $L_b(x) \in [b, \infty]$ and it increases on the interval $[0, \varepsilon]$.

- $Lim_{|x| \to \varepsilon} L_b(x) = +\infty$
- The function $L_b(x)$ exhibits a distinctive minimum point at zero.

In this study, the barrier function can be defined as follows

$$L_b(s) = \frac{\sqrt{\varepsilon}b}{(\varepsilon - |s|)^{\frac{1}{2}}}, \quad s \in (-\varepsilon, \varepsilon) \tag{17}$$

where b is a positive value and s is the sliding surface. According to [22], the variable gain $L(t, s)$ could be defined as follow:

$$L(t, s) = \begin{cases} \rho t + \varrho, & 0 \le t < t_1 \\ L_b(s), & t \ge t_1 \end{cases} \tag{18}$$

where t is time, ρ and ϱ are two positive numbers. For any $t > t_1$, $|s| < \varepsilon$ is satisfied.

IV. CONTROLER DESIGN AND STABILITY INVESTIGATION

In this section, an integrated terminal sliding mode control strategy is proposed. Inspired by [23], integral terminal sliding surfaces are designed as follows:

$$\begin{cases} s_1 = \alpha_1 e_1 + \dot{e}_1 + \beta_1 \int |s_1|^{\frac{\lambda_1 s_1^2}{1+\mu_1 s_1^2}} sign(s_1)\, dt \\ s_2 = \alpha_2 e_2 + \dot{e}_2 + \beta_2 \int |s_2|^{\frac{\lambda_2 s_2^2}{1+\mu_2 s_2^2}} sign(s_2)\, dt \\ s_3 = \alpha_3 e_3 + \dot{e}_3 + \beta_3 \int |s_3|^{\frac{\lambda_3 s_3^2}{1+\mu_3 s_3^2}} sign(s_3)\, dt \\ s_4 = \alpha_4 e_4 + \dot{e}_4 + \beta_4 \int |s_4|^{\frac{\lambda_1 s_4^2}{1+\mu_4 s_4^2}} sign(s_4)\, dt \end{cases} \tag{19}$$

which $\alpha_i (i = 1, 2, 3, 4)$ and $\beta_j (j = 1, 2, 3, 4)$ are positive values. λ_i and $\mu_i (i = 1, 2, 3, 4)$ are positive values with $\frac{\lambda_i}{\mu_i + 1} > 1$.

Taking the derivative of formula (19) yields formula (20) as follows

$$\begin{cases} \dot{s}_1 = \alpha_1 \dot{e}_1 + \ddot{e}_1 + \beta_1 |s_1|^{\frac{\lambda_1 s_1^2}{1+\mu_1 s_1^2}} sign(s_1) \\ \dot{s}_2 = \alpha_2 \dot{e}_2 + \ddot{e}_2 + \beta_2 |s_2|^{\frac{\lambda_2 s_2^2}{1+\mu_2 s_2^2}} sign(s_2) \\ \dot{s}_3 = \alpha_3 \dot{e}_3 + \ddot{e}_3 + \beta_3 |s_3|^{\frac{\lambda_3 s_3^2}{1+\mu_3 s_3^2}} sign(s_3) \\ \dot{s}_1 = \alpha_4 \dot{e}_4 + \ddot{e}_4 + \beta_4 |s_4|^{\frac{\lambda_4 s_4^2}{1+\mu_4 s_4^2}} sign(s_4) \end{cases} \tag{20}$$

Setting $\dot{s} = 0$ and submitting (12), (13), (14) and (15) into (20), the control laws can be expressed as follows:

$$\begin{cases} u_{2eq} = -\frac{1}{b_1}(a_1 x_4 x_6 + a_2 x_2^2 + a_3 \bar{\Omega} x_4 - \ddot{x}_{1d} + k_1 sign(s_1) \\ \qquad + \alpha_1 \dot{e}_1 + \beta_1 |s_1|^{\frac{\lambda_1 s_1^2}{1+\mu_1 s_1^2}} sign(s_1)) \\ u_{3eq} = -\frac{1}{b_2}(a_4 x_2 x_6 + a_5 x_4^2 + a_6 \bar{\Omega} x_2 - \ddot{x}_{2d} + k_2 sign(s_2) \\ \qquad + \alpha_2 \dot{e}_2 + \beta_2 |s_2|^{\frac{\lambda_2 s_2^2}{1+\mu_2 s_2^2}} sign(s_2)) \\ u_{4eq} = -\frac{1}{b_3}(a_7 x_2 x_4 + a_8 x_6^2 - \ddot{x}_{3d} + k_3 sign(s_3) + \alpha_3 \dot{e}_3 \\ \qquad + \beta_3 |s_3|^{\frac{\lambda_3 s_3^2}{1+\mu_3 s_3^2}} sign(s_3)) \\ u_{1eq} = -\frac{m}{cosx_1 cosx_3}(a_9 x_8 - g - \ddot{x}_{4d} + k_4 sign(s_4) + \alpha_4 \dot{e}_4 \\ \qquad + \beta_4 |s_4|^{\frac{\lambda_4 s_4^2}{1+\mu_4 s_4^2}} sign(s_4)) \end{cases} \tag{21}$$

where $k_i (i = 1, 2, 3, 4)$ are the positive values.

The switch control law can be designed as follows:

$$\begin{cases} u_{sw1} = -L_1 \sqrt{|s_1|} sign(s_1) - \int L_1^2 sign(s_1) dt \\ u_{sw2} = -L_2 \sqrt{|s_2|} sign(s_2) - \int L_2^2 sign(s_2) dt \\ u_{sw3} = -L_3 \sqrt{|s_3|} sign(s_3) - \int L_3^2 sign(s_3) dt \\ u_{sw4} = -L_4 \sqrt{|s_4|} sign(s_4) - \int L_4^2 sign(s_4) dt \end{cases} \tag{22}$$

where $\gamma_i (i = 1, 2, 3, 4)$ and $\eta_j (j = 1, 2, 3, 4)$ are all positive numbers.

Then, the design of the controller is as follows:

$$\begin{cases} u_2 = u_{2eq} + u_{sw1} \\ u_3 = u_{3eq} + u_{sw2} \\ u_4 = u_{4eq} + u_{sw3} \\ u_1 = u_{1eq} + u_{sw4} \end{cases} \tag{23}$$

The control flow chart of this paper is shown in Figure 1.

Theorem 1: Given the system (13) and the controller (23), the sliding surfaces (19) will converge to 0 in a finite time.

Proof 1: Choose the Lyapunov equation as follows:

$$\begin{cases} V_1 = \frac{1}{2} s_1^2 \\ V_2 = \frac{1}{2} s_2^2 \\ V_3 = \frac{1}{2} s_3^2 \\ V_4 = \frac{1}{2} s_4^2 \end{cases} \tag{24}$$

Differentiating V_1 with respect to time gives

$$\dot{V}_1 = s_1 \{\alpha_1 \dot{e}_1 + \ddot{e}_1 + \beta_1 |s_1|^{\frac{\lambda_1 s_1^2}{1+\mu_1 s_1^2}} sign(s_1)\} \tag{25}$$

Substituting Eq. (23) and (13) into Eq. (25) leads to

$$\begin{aligned} \dot{V}_1 = s_1(&-k_1 sign(s_1) - b_1 L_1 \sqrt{|s_1|} sign(s_1) \\ &- b_1 \int L_1^2 sign(s_1)\, dt) \end{aligned} \tag{26}$$

Since the barrier function L_1 is a piecewise function, the following proof is divided into two parts.

1) *When $0 \le t < t_1$, Eq. (26) can be written as follow:*

$$\begin{aligned} \dot{V}_1 &= s_1 \{-k_1 sign(s_1) - b_1(\rho_1 t + \varrho_1) \sqrt{|s_1|} sign(s_1) \\ &\quad - b_1 \int (\rho_1 t + \varrho_1)^2 sign(s_1)\, dt\} \\ &\le -\{k_1 |s_1| + b_1(\rho_1 t + \varrho_1) |s_1|^{\frac{3}{2}} \\ &\quad + b_1 |s_1| \int (\rho_1 t + \varrho_1)^2\, dt\} \end{aligned} \tag{27}$$

according to Definition 1, Eq. (13) and Eq. (21), we can get $k_1 > 0$, $b_1 > 0$, $\rho_1 > 0$ and $\varrho_1 > 0$. Thus, one can

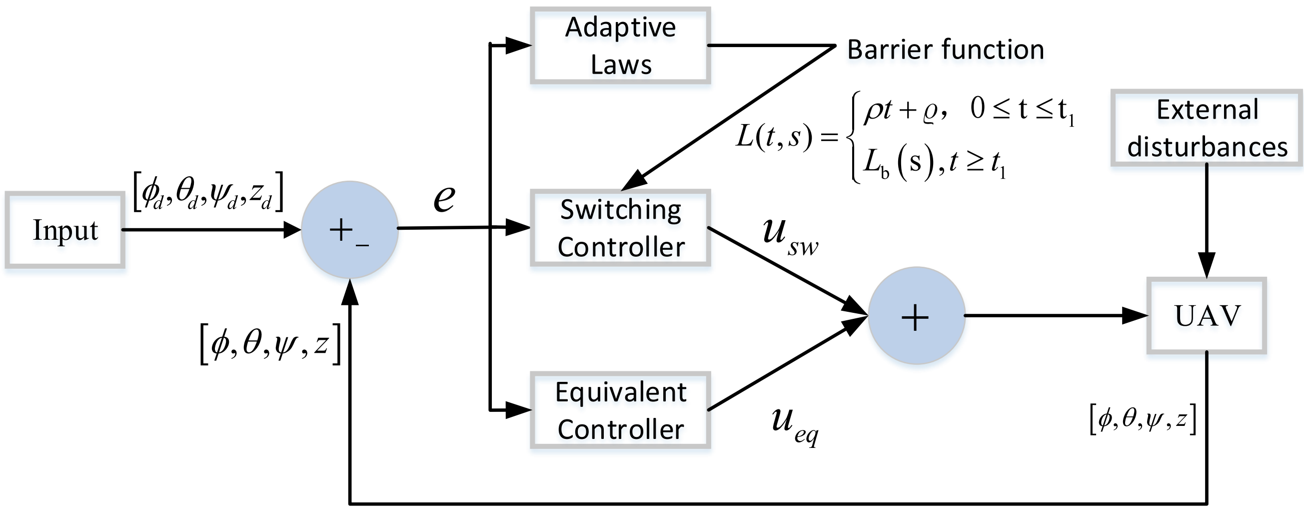

FIGURE 1. The control block diagram.

obtain

$$\dot{V}_1 \le -k_1|s_1| = -\sqrt{2}k_1(\frac{1}{2}s_1^2)^{\frac{1}{2}} = -\sqrt{2}k_1V_1^{\frac{1}{2}} \tag{28}$$

Let $\eta_1 = \sqrt{2}k_1$, we can get $t_n = \frac{2}{\eta_1}$. It means that s_1 converges to (-ε, ε) in finite time:

$$t_1 = t_0 + t_n \tag{29}$$

2) *When $t \ge t_1$, Eq. (26) can be written as follow:*

$$\begin{aligned}\dot{V}_1 &= s_1\{-k_1 sign(s_1) - b_1\frac{\sqrt{\varepsilon}b}{(\varepsilon-|s_1|)^{\frac{1}{2}}}\sqrt{|s_1|}sign(s_1)\\ &\quad - b_1\int(\frac{\sqrt{\varepsilon}b}{(\varepsilon-|s_1|)^{\frac{1}{2}}})^2 sign(s_1)\,dt\}\\ &\le -\{k_1|s_1| + b_1\frac{\sqrt{\varepsilon}b}{(\varepsilon-|s_1|)^{\frac{1}{2}}}|s_1|^{\frac{3}{2}}\\ &\quad + b_1|s_1|\int\frac{\varepsilon b^2}{(\varepsilon-|s_1|)}dt\}\\ &\le -\{k_1|s_1| + b_1\frac{\sqrt{\varepsilon}b}{(\varepsilon-|s_1|)^{\frac{1}{2}}}|s_1|^{\frac{3}{2}}\}\\ &\le -\{k_1|s_1| + bb_1|s_1|^{\frac{3}{2}}\}\\ &= -\sqrt{2}k_1V_1^{\frac{1}{2}} - bb_1 2^{\frac{3}{4}}V_1^{\frac{3}{4}}\end{aligned} \tag{30}$$

We can obtain that $\dot{V}_1 < 0$. Let $\eta_2 = \sqrt{2}k_1$, $\eta_3 = bb_1 2^{\frac{3}{4}}$, $t_m = \frac{2}{\eta_2} + \frac{4}{\eta_3}$. The function $\dot{V}_1$ will converge to zero in a finite time at the initial time t_1:

$$t_s = t_1 + t_m \tag{31}$$

To sum up, $\dot{V}_1 < 0$ is negative definite, which means that V_1 and s_1 are both bounded. In the same way, $\dot{V}_2$, $\dot{V}_3$ and $\dot{V}_4$ are all negative definite. The integral terminal sliding mode controller enables the system to achieve optimal trajectory characteristics and guarantees the global asymptotic stability of the closed-loop control system.

V. SIMULATION EXPERIMENT

The system parameters are given in Table 1.

TABLE 1. The system parameters.

Parameter	Value	Parameter	Value
m(Kg)	0.486	K_{faz}(N/rad/s)	6.3540e-4
d(m)	0.25	K_{fdx}(N/m/s)	5.5670e-4
I_x(N m/rad/s^2)	3.8278e-3	K_{fdy}(N/m/s)	5.5670e-4
I_y(N m/rad/s^2)	3.8278e-3	K_{fdz}(N/m/s)	6.3540e-4
I_z(N m/rad/s^2)	7.6566e-3	K_P(N m/rad/s)	2.9842e-3
K_{fax}(N/rad/s)	5.5670e-4	C_d(N m/rad/s)	3.2320e-2
K_{fay}(N/rad/s)	5.5670e-4	J_r(N m/rad/s^2)	2.8385e-5

Remark 1: To adjust the parameters of the controller (23), some guidelines are provided below:

- choose t_1 according to characteristics of sliding surface;
- take $k_i > 0$ with $|k_i| > |d_j|$(i=1,2,3,4;j=ϕ, θ, ψ, z);
- barrier function parameters ε, b, ρ_i, $\varrho_j(i,j = 1,2,3,4)$ are determined by trial and error.

1) *Trajectory tracking experiment*
The initial state of the quad-rotor UAV system is selected as $x_i = 1(i = 1\ldots8)$. The external disturbances are selected as $d_\phi = 0.5sin(4t)$, $d_\theta = 0.5cos(4t)$, $d_\psi = 0.5sin(8t)$, $d_z = 0.5cos(8t)$. $\alpha_i = 10(i = 1,2,3,4)$, $\beta_1 = \beta_2 = \beta_3 = 0.1$ and $\beta_4 = 0.01$, $\lambda_i = 5(i = 1,2,3,4)$ and $\mu_i = 3.5(i = 1,2,3,4)$ are selected as the sliding surface parameters. The gains of the controllers are chosen as $k_i = 5(i = 1,2,3,4)$. $t_1 = 1.5$, $\varepsilon = 0.1$, $b = 1$, $\rho_1 = \rho_2 = \rho_3 = 2$, $\rho_4 = 3$, $\varrho_1 = \varrho_2 = \varrho_3 = 0.5$ and $\varrho_4 = 1.5$ are the barrier function parameters. $x_{1d} = sin(5t)$, $x_{2d} = cos(5t)$,

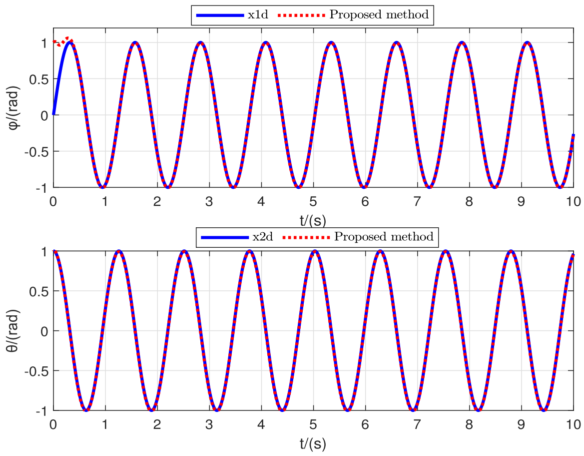

FIGURE 2. ϕ **(roll angle) and** θ **(pitch angle) tracking results.**

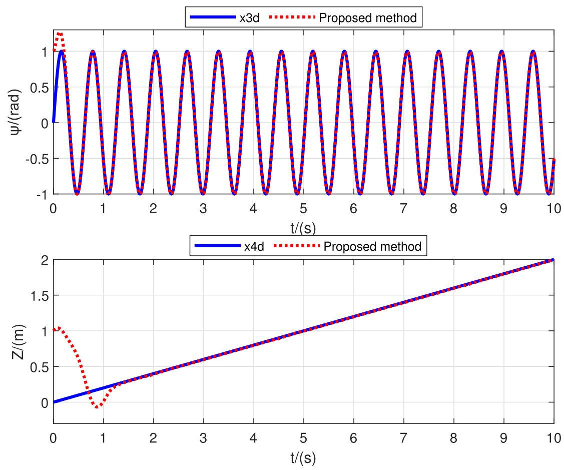

FIGURE 3. ψ **(yaw angle) and** z **(altitude) tracking results.**

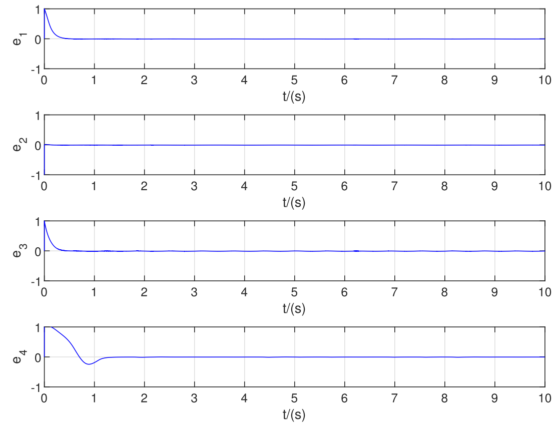

FIGURE 4. ϕ**,** θ**,** ψ **and** z **tracking errors.**

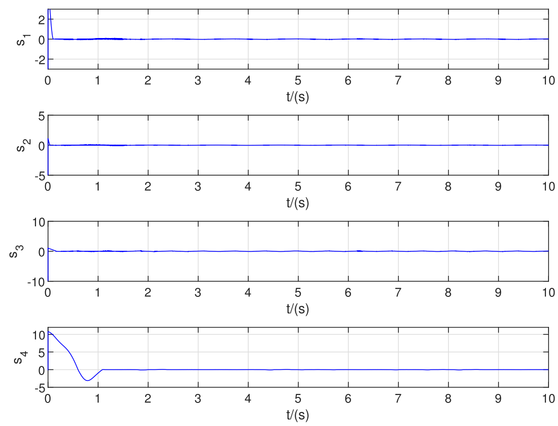

FIGURE 5. The sliding surfaces.

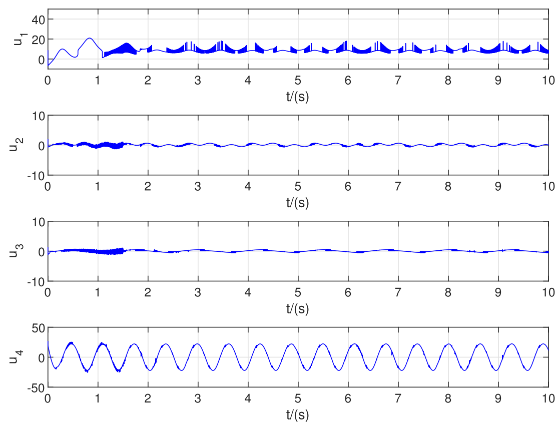

FIGURE 6. The control signals.

$x_{3d} = sin(10t)$ and $x_{4d} = 0.2t$ are the desired trajectories.

Figure 2 illustrates the impact of roll angle and pitch angle on track tracking. In this figure, it is evident that within a time range of approximately 0.5 seconds and 0.1 seconds, the trajectories of roll angle and pitch angle accurately follow the expected trajectory. Figure 3 illustrates the impact of yaw angle and altitude on track tracking. The figure indicates that the yaw angle achieves tracking of the desired trajectory at 0.5 seconds, while the altitude achieves tracking of the desired trajectory at 1.3 seconds.

Figure 4 illustrates the discrepancy in tracking accuracy between the desired trajectory and the actual trajectory. From the graph, it is evident that the errors of all four trajectories exhibit a rapid convergence towards zero when tracked concurrently. The state remains stable once the tracking error reaches a convergence of 0. This validates the capability of the proposed methodology to efficiently mitigate external disturbances and affirms the efficacy of this approach. Figure 5 shows the sliding surfaces, which could converge to 0 in a short time. Figure 6 depicts the control signals.

2) *Contrast experiment*

The desired trajectories are selected as $x_{1d} = sin(t)$, $x_{2d} = sin(2t)$, $x_{3d} = 2sin(t)$ and $x_{4d} = 0.1t$, all other parameters are consistent with the parameters of the

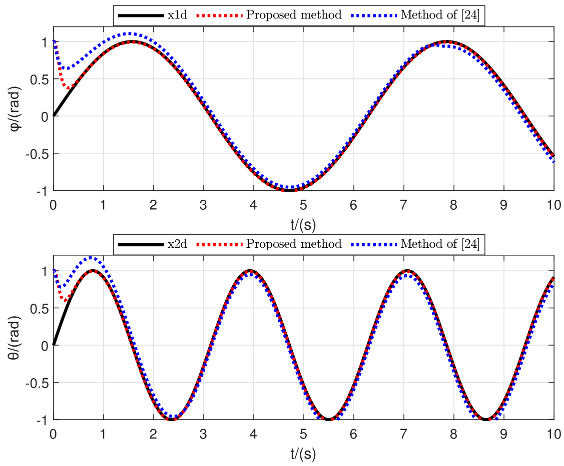

FIGURE 7. ϕ **(roll angle) and** θ **(pitch angle) compare tracking results.**

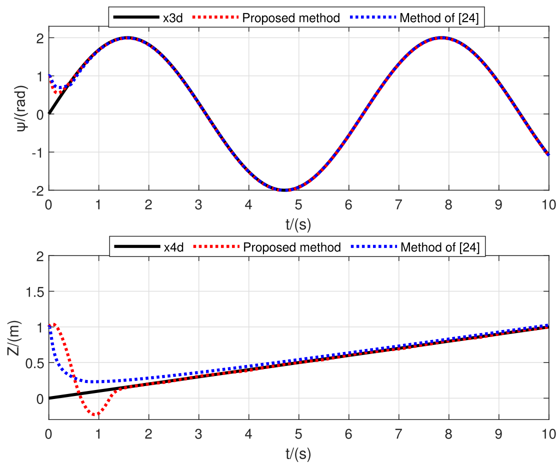

FIGURE 8. ψ **(yaw angle) and** z **(altitude) compare tracking results.**

previous experimentand, and the proposed method is also compared with the method of [24].

Figures 7 and 8 show the comparative tracking results for the four degrees of freedom of the quad-rotor UAV ϕ (roll angle), θ (pitch angle), ψ (yaw angle), and z (altitude), respectively. It can be clearly observed in the figures that the proposed method can track the desired trajectory quickly and accurately. However, using the methods in [24], there is a certain deviation from the desired trajectory, and the tracking speed is slower than that of the method proposed in this paper.

Figure 9 shows the tracking errors of using the proposed method and method of [24]. The convergence speed of e_1 and e_2 is significantly faster than that of the method in [24], and the convergence accuracy is also higher than that of the method in [24]. e_3 and e_4 converge to 0 significantly faster than the method in [24]. In addition, it can be clearly seen in Figure 9 that the tracking error of the proposed method is

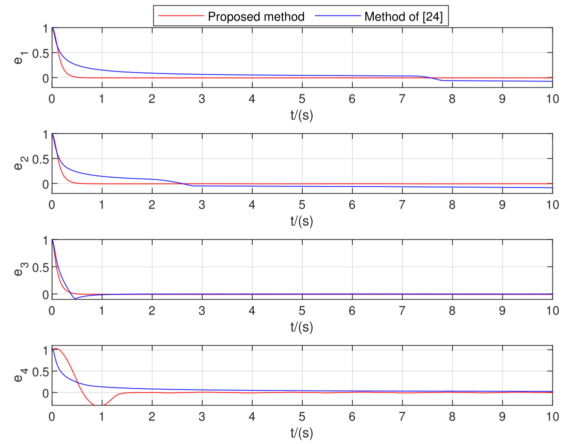

FIGURE 9. ϕ**,** θ**,** ψ **and** z **compare tracking errors.**

significantly smaller than that of the method in [24], which proves the superiority of the proposed method.

In summary, the simulation experiments validate the effectiveness and robustness of the proposed barrier function-based super-twisting integral terminal sliding mode control strategy. Super-twisting algorithm has the ability to effectively reduce the chattering of the sliding surface. The implementation of the barrier function strategy guarantees that as the derivatives of disturbances increase, the super-twisting gains also increase to ensure that the output value remains within the desired vicinity before gradually decreasing. The above two strategies effectively improve control performance.

VI. CONCLUSION

In this article, a barrier function-based super-twisting integral terminal sliding mode control strategy is proposed for altitude and attitude control of quad-rotor UAVs. The integral term of sliding mode ensures that the system's initial state lies on the sliding surface from the beginning, thereby eliminating the reachable segment. Additionally, incorporating an exponential component enhances the speed at which the system state converges. The super-twisting algorithm is implemented to mitigate the chattering issue associated with the sliding mode control approach while utilizing the barrier function as the gain of the super-twisting algorithm to further enhance the robustness of the control system. Moreover, the algorithm neither requires an upper bound on the derivative of the perturbation nor uses a low-pass filter, which ensures that once the derivative of the perturbation increases, the overtwist gain also increases, thus ensuring that the output value belongs to the desired neighborhood. Finally, the proposed method is validated and proven to be effective and superior through simulation experiments.

For future work, although the sliding mode control strategy is robust to model uncertainty, there are still adverse effects. References [25], [26], and [27] combine neural networks with sliding mode control to effectively avoid the impact of model uncertainty. Therefore, inspired by the above articles, the next step is to combine the neural network with the method proposed in this paper, which should be applied in practice.

ACKNOWLEDGMENT
The author would like to thank the unidentified reviewers for their valuable feedback, which has contributed significantly to enhancing the overall caliber of this manuscript.

REFERENCES
[1] W. Liu, T. Zhang, S. Huang, and K. Li, "A hybrid optimization framework for UAV reconnaissance mission planning," *Comput. Ind. Eng.*, vol. 173, Nov. 2022, Art. no. 108653.
[2] Z. Li, Q. Wang, T. Zhang, C. Ju, S. Suzuki, and A. Namiki, "UAV high-voltage power transmission line autonomous correction inspection system based on object detection," *IEEE Sensors J.*, vol. 23, no. 9, pp. 10215–10230, May 2023.
[3] J. Su, X. Zhu, S. Li, and W.-H. Chen, "AI meets UAVs: A survey on AI empowered UAV perception systems for precision agriculture," *Neurocomputing*, vol. 518, pp. 242–270, Jan. 2023.
[4] J. Hu, H. Niu, J. Carrasco, B. Lennox, and F. Arvin, "Fault-tolerant cooperative navigation of networked UAV swarms for forest fire monitoring," *Aerosp. Sci. Technol.*, vol. 123, Apr. 2022, Art. no. 107494.
[5] M. M. Azari, G. Geraci, A. Garcia-Rodriguez, and S. Pollin, "UAV-to-UAV communications in cellular networks," *IEEE Trans. Wireless Commun.*, vol. 19, no. 9, pp. 6130–6144, Sep. 2020.
[6] C. Zhang, L. Zhang, L. Zhu, T. Zhang, Z. Xiao, and X.-G. Xia, "3D deployment of multiple UAV-mounted base stations for UAV communications," *IEEE Trans. Commun.*, vol. 69, no. 4, pp. 2473–2488, Apr. 2021.
[7] D. Yan, W. Zhang, H. Chen, and J. Shi, "Robust control strategy for multi-UAVs system using MPC combined with Kalman-consensus filter and disturbance observer," *ISA Trans.*, vol. 135, pp. 35–51, Apr. 2023.
[8] J. Li, G. Zhang, Q. Shan, and W. Zhang, "A novel cooperative design for USV-UAV systems: 3D mapping guidance and adaptive fuzzy control," *IEEE Trans. Control Netw. Syst.*, pp. 1–11, Nov. 2022.
[9] K. Liu, R. Wang, X. Wang, and X. Wang, "Anti-saturation adaptive finite-time neural network based fault-tolerant tracking control for a quadrotor UAV with external disturbances," *Aerosp. Sci. Technol.*, vol. 115, Aug. 2021, Art. no. 106790.
[10] G. Wen, W. Hao, W. Feng, and K. Gao, "Optimized backstepping tracking control using reinforcement learning for quadrotor unmanned aerial vehicle system," *IEEE Trans. Syst. Man, Cybern., Syst.*, vol. 52, no. 8, pp. 5004–5015, Aug. 2022.
[11] Z. Hou, P. Lu, and Z. Tu, "Nonsingular terminal sliding mode control for a quadrotor UAV with a total rotor failure," *Aerosp. Sci. Technol.*, vol. 98, Mar. 2020, Art. no. 105716.
[12] X. Shao, G. Sun, W. Yao, J. Liu, and L. Wu, "Adaptive sliding mode control for quadrotor UAVs with input saturation," *IEEE/ASME Trans. Mechatronics*, vol. 27, no. 3, pp. 1498–1509, Jun. 2022.
[13] J. Baek and M. Kang, "A synthesized sliding-mode control for attitude trajectory tracking of quadrotor UAV systems," *IEEE/ASME Trans. Mechatronics*, pp. 1–11, Jan. 2022.
[14] Y. Ma, D. Li, Y. Li, and L. Yang, "A novel discrete compound integral terminal sliding mode control with disturbance compensation for PMSM speed system," *IEEE/ASME Trans. Mechatronics*, vol. 27, no. 1, pp. 549–560, Feb. 2022.
[15] T. Yang, Y. Deng, H. Li, Z. Sun, H. Cao, and Z. Wei, "Fast integral terminal sliding mode control with a novel disturbance observer based on iterative learning for speed control of PMSM," *ISA Trans.*, vol. 134, pp. 460–471, Mar. 2023.
[16] N. P. Nguyen, H. Oh, and J. Moon, "Continuous nonsingular terminal sliding-mode control with integral-type sliding surface for disturbed systems: Application to attitude control for quadrotor UAVs under external disturbances," *IEEE Trans. Aerosp. Electron. Syst.*, vol. 58, no. 6, pp. 5635–5660, Dec. 2022.
[17] M. Rahmani, A. Ghanbari, and M. M. Ettefagh, "Hybrid neural network fraction integral terminal sliding mode control of an inchworm robot manipulator," *Mech. Syst. Signal Process.*, vol. 80, pp. 117–136, Dec. 2016.
[18] A. Levant, "Robust exact differentiation via sliding mode technique," *Automatica*, vol. 34, no. 3, pp. 379–384, Mar. 1998.
[19] Y. Qin, J. J. Rath, C. Hu, C. Sentouh, and R. Wang, "Adaptive nonlinear active suspension control based on a robust road classifier with a modified super-twisting algorithm," *Nonlinear Dyn.*, vol. 97, no. 4, pp. 2425–2442, Sep. 2019.
[20] D. Ashtiani Haghighi and S. Mobayen, "Design of an adaptive super-twisting decoupled terminal sliding mode control scheme for a class of fourth-order systems," *ISA Trans.*, vol. 75, pp. 216–225, Apr. 2018.
[21] S. Mobayen, F. Tchier, and L. Ragoub, "Design of an adaptive tracker forn-link rigid robotic manipulators based on super-twisting global nonlinear sliding mode control," *Int. J. Syst. Sci.*, vol. 48, no. 9, pp. 1990–2002, Jul. 2017.
[22] H. Obeid, S. Laghrouche, L. Fridman, Y. Chitour, and M. Harmouche, "Barrier function-based adaptive super-twisting controller," *IEEE Trans. Autom. Control*, vol. 65, no. 11, pp. 4928–4933, Nov. 2020.
[23] O. Mofid and S. Mobayen, "Adaptive sliding mode control for finite-time stability of quad-rotor UAVs with parametric uncertainties," *ISA Trans.*, vol. 72, pp. 1–14, Jan. 2018.
[24] H. Ghadiri, M. Emami, and H. Khodadadi, "Adaptive super-twisting non-singular terminal sliding mode control for tracking of quadrotor with bounded disturbances," *Aerosp. Sci. Technol.*, vol. 112, May 2021, Art. no. 106616.
[25] J. Fei, Z. Wang, and Q. Pan, "Self-constructing fuzzy neural fractional-order sliding mode control of active power filter," *IEEE Trans. Neural Netw. Learn. Syst.*, pp. 1–12, May 2022.
[26] J. Fei and L. Liu, "Fuzzy neural super-twisting sliding-mode control of active power filter using nonlinear extended state observer," *IEEE Trans. Syst. Man, Cybern., Syst.*, vol. 54, no. 1, pp. 457–470, Jan. 2024.
[27] J. Fei, L. Zhang, J. Zhuo, and Y. Fang, "Wavelet fuzzy neural supertwisting sliding mode control of an active power filter," *IEEE Trans. Fuzzy Syst.*, vol. 31, no. 11, pp. 4051–4063, Nov. 2023.

XINXIN CHEN received the B.S. degree in automation from Northeastern University, Shenyang, China, in 2006, and the M.S. degree in mechanical engineering from Wuyi University, Jiangmen, China, in 2009.

Since 2010, she has been an Associate Professor with the Guangdong Technology College. Her research interests include chaotic synchronization control systems and sliding mode control theory.